

Cite this: *CrystEngComm*, 2012, **14**, 2229

www.rsc.org/crystengcomm

PAPER

Template-free synthesis of monodisperse α -Fe₂O₃ porous ellipsoids and their application to gas sensors

Peng Sun, Xinxin He, Wenbo Wang, Jian Ma, Yanfeng Sun* and Geyu Lu*

Received 21st October 2011, Accepted 6th December 2011

DOI: 10.1039/c2ce06400f

Monodisperse porous α -Fe₂O₃ ellipsoids composed of primary nanocrystals were synthesized by a facile one-step template-free hydrothermal method. Field emission scanning electron microscopic and transmission electron microscopic results revealed that these porous ellipsoids were built from a large number of nanoparticles with sizes of about 10–20 nm. The morphology and size of the as-prepared products could be tailored by simply adjusting the amounts of hexamethylenetetramine and reaction temperature. A possible formation mechanism was proposed on the basis of the results of time-dependent experiments. When used as sensing materials in chemical sensors, the as-prepared porous α -Fe₂O₃ ellipsoids exhibit a high response to ethanol.

Introduction

As one of the most important multifunctional metal oxides, α -Fe₂O₃ has been considered an ideal material for chemical sensors,^{1–3} magnetic devices,⁴ catalysis,⁵ and water splitting *etc.*⁶ due to its non-toxicity, low cost, and relatively good stability. In order to highlight some special properties demanded by particular technological applications, various α -Fe₂O₃ with different dimensional nanostructures have been synthesized, including nanoparticles (0 D),⁷ rods, wires, and tubes (1 D),^{8–10} disks, sheets, and rings (2D),^{11–13} urchin-like, and dendrites (3 D).^{14,15}

Recently, porous and hollow inorganic nanostructures have attracted considerable attention because of their low density, large surface area, stability, and surface permeability. Such materials have potential applications in a number of areas including chemical reactors,¹⁶ sensors,¹⁷ drug delivery,¹⁸ and catalysis *etc.*¹⁹ Currently, a common synthetic strategy for the preparation of porous and hollow structures is the utilization of various removable or sacrificial templates, referred to as “hard”, such as monodispersed silica,²⁰ polymer latex spheres,²¹ and reducing metal nanoparticles,²² as well as “soft” ones, for example, emulsion droplets/micelles,²³ and gas bubbles.²⁴ However, porous and hollow structures prepared from hard template-assisted routes usually suffer from disadvantages related to high cost and tedious synthetic procedures, which may prevent them from being used in large-scale applications. Therefore, a facile, and economical route to rationally prepare porous and hollow structures with controllable shapes, and porous sizes is still a challenge and highly desirable. Recently,

lots of one-step template-free methods for synthesizing porous and hollow inorganic nanostructures have been developed employing novel mechanisms, including Ostwald ripening,^{25–30} Kirkendall effect,^{31,32} and oriented attachment.^{33,34}

In this paper, we report the synthesis of monodisperse porous α -Fe₂O₃ ellipsoids by a facile one-step template-free hydrothermal method. The synthesis was performed in an ethanol–water mixed solvent using ferric trichloride as the precursor. It was found that amounts of hexamethylenetetramine (HMT) and hydrothermal temperature played an important role in controlling the morphology and size of the α -Fe₂O₃ microcrystals. Moreover, the formation process had been investigated through the morphology evolution with different reaction times, and a possible formation mechanism was speculated. The gas sensing properties of the sensors based on the synthesized porous α -Fe₂O₃ ellipsoids exhibited a high response to ethanol. The excellent gas sensing properties are attributed to the high porosity of the α -Fe₂O₃ ellipsoids.

Experimental

Synthesis of flower-like α -Fe₂O₃ nanorods

Monodisperse porous α -Fe₂O₃ ellipsoids were synthesized by a simple hydrothermal method. All the reagents in the experiment were of analytical grade (Beijing Chemicals Co., Ltd.) and were used as received without further purification. In a typical experiment, 4.054 g FeCl₃·6H₂O was dissolved in a 30 mL water–ethanol mixture (1 : 1, v/v) under magnetic stirring. Then 0.2 g (CH₂)₆N₄ (HMT) was added into the above solution. After several minutes of ultrasonic dispersing, the mixture was transferred into a Teflon-lined stainless steel autoclave, maintained at 160 °C for 12 h, and allowed to cool to room temperature naturally. The resulting precipitates were collected by

State Key Laboratory on Integrated Optoelectronics, College of Electronic Science and Engineering, Jilin University, Changchun, 130012, People's Republic of China. E-mail: luyg@jlu.edu.cn; syf@jlu.edu.cn; Fax: +86 431 85167808; Tel: +86 431 85167808

centrifugation, washed several times with deionized water and ethanol, and finally dried *in vacuo* at 80 °C for 6 h.

Characterization of samples

Powder X-ray diffraction (XRD) pattern was recorded with a Rigaku D/max-2500 diffractometer using Cu-K α radiation. Field-emission scanning electron microscopy (FESEM) observations were carried out using a JEOL JSM-7500F microscope with an accelerating voltage of 15 kV. Transmission electron microscopy (TEM) selected-area electron diffraction (SAED), and high-resolution transmission electron microscopy (HRTEM) measurements were conducted using a TECNAIF 20 microscope with an accelerating voltage of 200 kV. The specific surface area was estimated using the Brunauer-Emmett-Teller (BET) equation based on the nitrogen adsorption isotherm obtained with a Micromeritics Gemini VII apparatus (Surface Area and Porosity System). The sample was degassed under vacuum at 250 °C for 12 h prior to the measurements.

Measurement of ethanol sensing properties

Gas sensors were fabricated as follows: the synthesized porous α -Fe₂O₃ were mixed with deionized water, and then coated onto an alumina tube, on which a pair of gold electrodes was installed at each end, and each electrode was connected with a Pt wire. A Ni-Cr alloy coil was inserted to the alumina tube as a heater, allowing us to control the operating temperature of sensors. The gas-sensing properties of the samples were evaluated with a RQ-2 gas-sensing characterization system. The measurement was processed by a static process: a given amount of the tested gas was injected into a closed glass chamber, and the sensor was put into the chamber for the measurement of the sensing performance. The gas response was defined as R_a/R_g , where R_a and R_g are the resistances measured in air and the tested gas atmosphere. The response and recovery times were defined as the time taken by the sensor to achieve 90% of the total resistance change in the case of adsorption and desorption, respectively.

Results and discussion

The powder prepared with 0.2 g was characterized by X-ray diffraction to identify its structure and the diffraction pattern is shown in Fig. 1. All of the diffraction peaks could be indexed well to the standard α -Fe₂O₃ according to JCPDS card No. 33-0664, with space group $R\bar{3}c$ and lattice parameters of $a = 5.035$ Å and $c = 13.75$ Å. No diffraction peaks from any other impurities were observed.

The morphologies and microstructures of the α -Fe₂O₃ products obtained with 0.2 g HMT at 160 °C for 12 h are illustrated by FESEM and TEM observations. A panoramic FESEM image of the as-prepared α -Fe₂O₃ is shown in Fig. 2a, from which a number of uniform and monodisperse ellipsoids were clearly observed. No other morphologies could be detected, indicating a high yield of these ellipsoids. It can be observed from the enlarged FESEM image of Fig. 2b that the diameters of the obtained α -Fe₂O₃ ellipsoid along the long and short axis directions were 1.5 μ m and 1 μ m respectively. The high-magnification FESEM image shows the detailed morphologies of the α -Fe₂O₃ ellipsoids. Apparently, the rough and porous surfaces of the

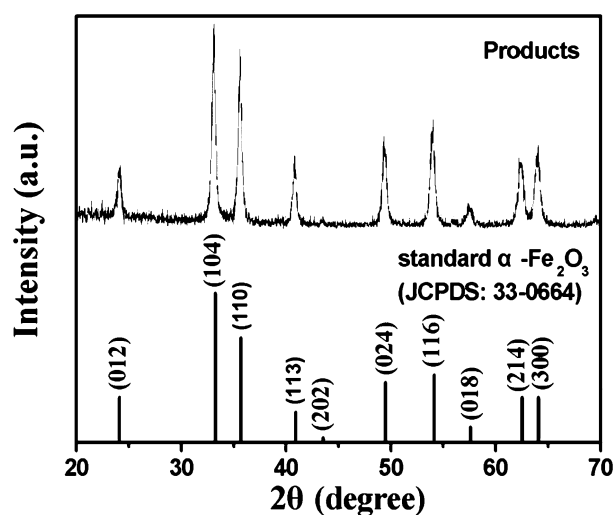


Fig. 1 X-ray diffraction pattern of porous α -Fe₂O₃ ellipsoids obtained with 0.2 g HMT at 160 °C for 12 h and the standard XRD pattern of α -Fe₂O₃ (JCPDS No. 33-0664).

elliptical structures were exhibited (Fig. 2c and the inset). A broken α -Fe₂O₃ ellipsoid is shown in Fig. 2d, indicating that the ellipsoid was formed entirely by aggregated small primary α -Fe₂O₃ nanoparticles with a diameter of 20 nm. This hierarchical α -Fe₂O₃ nanostructure may be suitable to gas sensing applications due to their porosity.

In addition, further detailed structural analysis of the porous ellipsoids was carried out using TEM and HRTEM. The typical TEM images of porous ellipsoids prepared with 0.2 g HMT at 160 °C for 12 h in Fig. 3a show that the size and shape of α -Fe₂O₃ ellipsoids were similar to those of FESEM observations. Moreover, the TEM image of an individual α -Fe₂O₃ ellipsoid (the inset in Fig. 3a) further clearly displays the porous structures of the α -Fe₂O₃ ellipsoids. The corresponding SAED pattern (the inset in Fig. 3a) confirms that the hierarchical α -Fe₂O₃ ellipsoids were polycrystalline structures in nature. However, the pattern was not a ring, which indicates that the ellipsoid should consist of

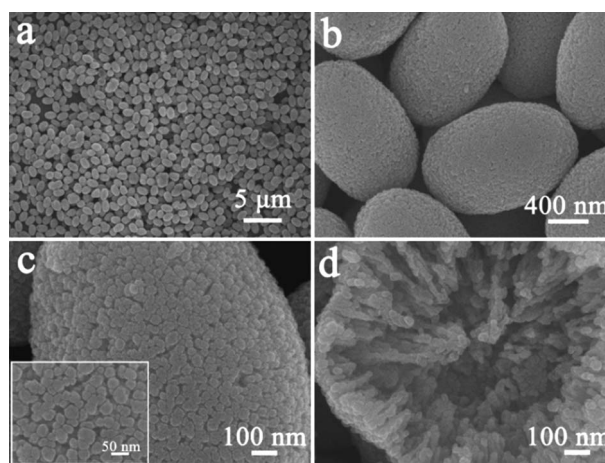


Fig. 2 Morphological characterization of the α -Fe₂O₃ products prepared with 0.2 g HMT at 160 °C for 12 h: (a) panoramic, (b) enlarged, and (c-d) high-magnification FESEM images. The inset of (c) is an image of selective area magnification.

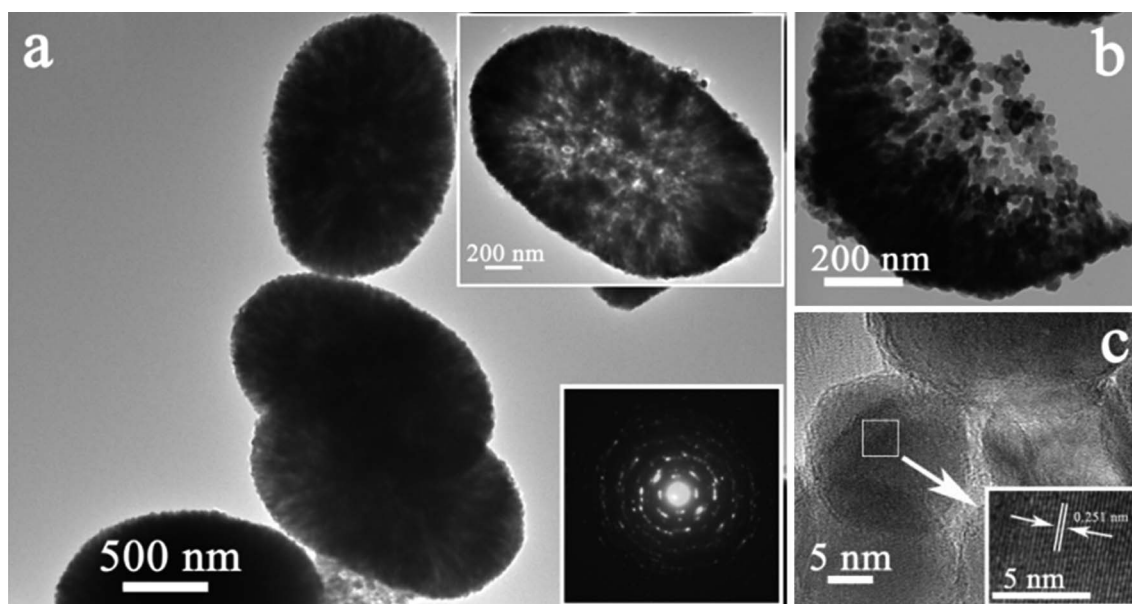


Fig. 3 (a) TEM images and SAED pattern of α -Fe₂O₃ ellipsoid synthesized with 0.2 g HMT at 160 °C for 12 h. (b) Typical TEM image of a broken α -Fe₂O₃ ellipsoid. (c) HRTEM image of α -Fe₂O₃ nanoparticles. Inset: enlarged HRTEM image obtained from the marked fringe of nanoparticle.

single-crystal building blocks. Fig. 3b presents a broken ellipsoid. It can be seen that the ellipsoid was composed of a large number of nanoparticles, in accordance with the FESEM image (Fig. 2d). The HRTEM image shown in Fig. 3c indicates that the diameters of nanoparticles were about 20 nm. The inset in Fig. 3c shows the HRTEM image obtained from the marked fringe of the α -Fe₂O₃ nanoparticles in Fig. 3c, from which the lattice fringes could be observed clearly and the lattice spacing was 0.251 nm, corresponding to the (110) plane of α -Fe₂O₃. The result confirms the single-crystal structure of nanoparticles.

To further confirm the inner architectures of the porous α -Fe₂O₃ ellipsoids, N₂ adsorption and desorption measurements were carried out. The typical adsorption and desorption isotherm and the corresponding Barrett–Joyner–Halenda (BJH) pore size distribution curve of the porous α -Fe₂O₃ ellipsoids are shown in Fig. 4 and the inset. According to the IUPAC classification, the loop observed was ascribed to a type IV isotherm with a type H3 hysteresis loop, indicating the existence of mesopores (pores 2–50 nm in diameter) in the material. Using the BJH method and the desorption branch of the nitrogen isotherm, the calculated pore-size distribution indicated that the material contained an average pore size of 14 nm. Such porous structures provide efficient transport pathways for effective gas diffusion to the interior of ellipsoids, which would enhance the gas sensing performance of sensor. Moreover, the BET surface area of the products was calculated to be 25 m² g⁻¹.

The influences of experimental parameters on the microstructures of final as-prepared products were investigated systemically. The results show that the amounts of HMT and hydrothermal temperature played important roles in controlling the morphologies and sizes of the α -Fe₂O₃ microcrystals. Keeping other conditions unchanged, in the absence of HMT, the resultant products consisted of compact-aggregated particles with a wide size distribution (Fig. 5a). These particles transformed into the uniform porous ellipsoids (Fig. 5b and the inset)

with the introduction of HMT (0.2 g) into the solution. As the amount of HMT was increased to 0.6 g, the quasi-cubic particles were formed with coarse surfaces and a size of about 800 nm (Fig. 5c). With a further increase of HMT (1.2 g), the quasi-cubic structure of α -Fe₂O₃ evolved into regular cubic shape, and craterlets in the surfaces of the cubes could be observed (Fig. 5d). The inset of Fig. 5d shows the image of a broken cube indicating that the cube was a porous structure. Therefore, on the basis of the morphological study, it can be concluded that HMT plays an important role in forming porous α -Fe₂O₃ ellipsoids.

Apart from the HMT amount, the temperature of the hydrothermal reaction was another synthetic parameter that had a significant effect on the as-prepared α -Fe₂O₃ products. The

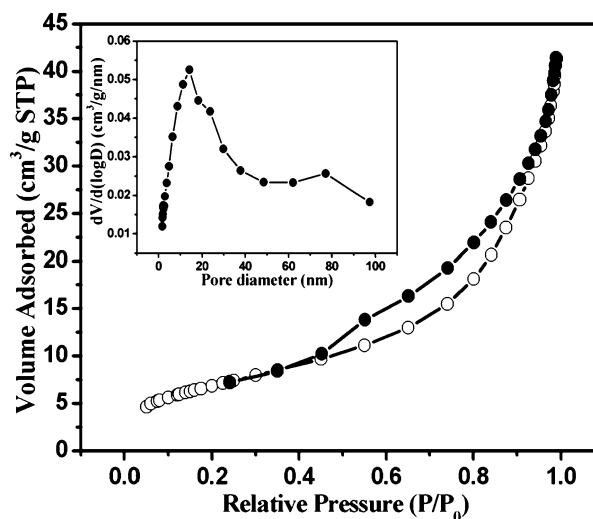


Fig. 4 Typical nitrogen adsorption–desorption isotherm and BJH pore size distribution plot (inset) of porous α -Fe₂O₃ ellipsoids prepared with 0.2 g HMT at 160 °C for 12 h.

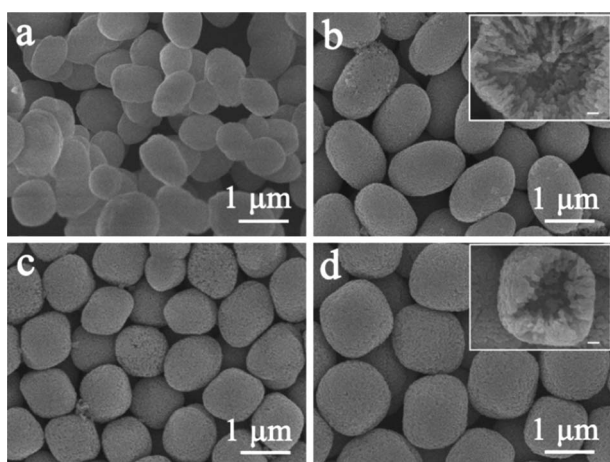


Fig. 5 FESEM images of α - Fe_2O_3 particles obtained with different HMT amounts at 160 °C for 12 h: (a) 0.0, (b) 0.2, (c) 0.6, and (d) 1.2 g. The insets of b and d show the enlarged image, and scale bars are 100 nm.

product synthesized at 140 °C consisted of monodisperse ellipsoids with smooth surfaces and the diameters of 800 nm and 1 μm along the long and short axis directions (Fig. 6a and the inset), respectively. A further increase of the hydrothermal temperature to 160 °C led to the formation of porous ellipsoids. The detailed morphology characteristics of them are described previously (Fig. 6b and the inset). By increasing the temperature to 180 °C (Fig. 6c and the inset), the as-prepared product consisted of a large scale of rugged and broken ellipsoids, which confirmed that these ellipsoids were indeed porous structures. As for the size, the product at 180 °C was smaller than that at 160 °C. Moreover, the enlarged inset indicated that the porous ellipsoids are composed of numerous compact-aggregated nanoparticles.

To reveal the growth process of porous α - Fe_2O_3 ellipsoids and possible growth mechanism, the study of the morphology evolution of α - Fe_2O_3 ellipsoids with different reaction times have been conducted. The corresponding results are shown in Fig. 7. When the hydrothermal time was 1 h, it can be seen that the product was entirely comprised of relatively uniform nanorods (Fig. 7a). With the reaction time increasing to 2 h, these nanorods transformed into uneven elliptic particles with smooth surfaces (Fig. 7b). As the hydrothermal process was prolonged to 3 h, FESEM images show that these elliptic particles sizes became relatively homogeneous. The diameters of the ellipsoids along the long and short axis directions were 600 nm and 1 μm respectively (Fig. 7c). With the reaction time increasing to 6 h, the

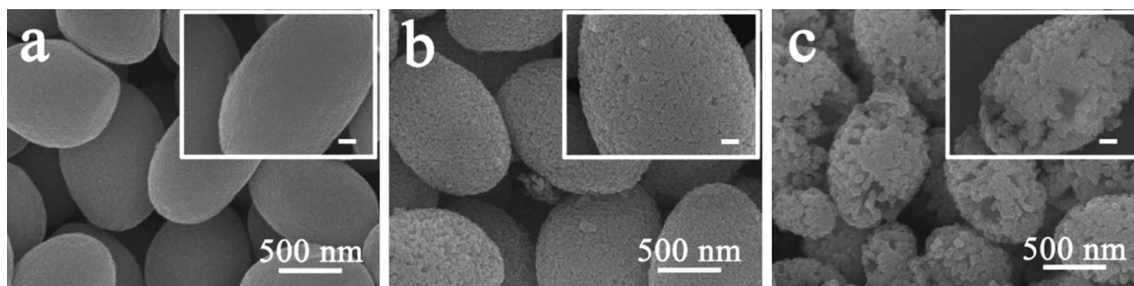


Fig. 6 FESEM images of products synthesized with 0.2 g HMT at (a) 140 °C, (b) 160 °C, and (c) 180 °C for 12 h. The insets are corresponding high-magnification images. Scale bars are 100 nm.

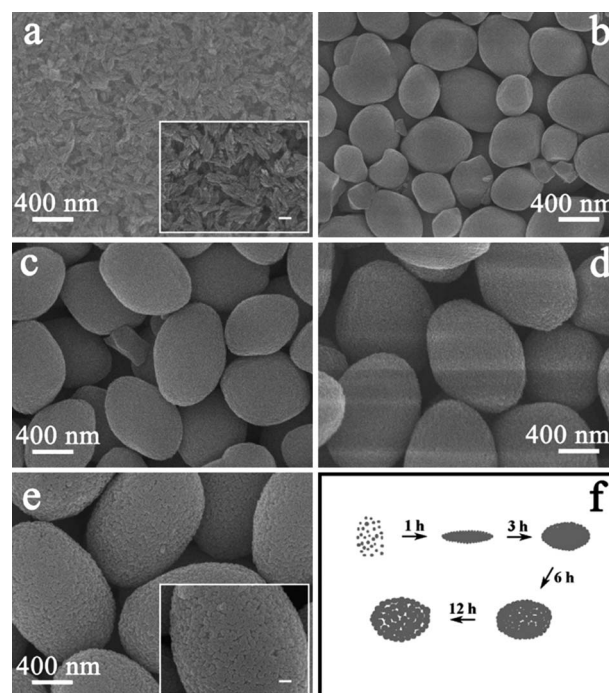


Fig. 7 FESEM images of morphology evolution of α - Fe_2O_3 nanostructures prepared with 0.2 g HMT at 160 °C for different reaction times: (a) 1 h, (b) 2 h, (c) 3 h, (d) 6 h, (e) 12 h. The insets show the enlarged images, and the scale bar is 100 nm. (f) Schematic illustration of the formation process of porous α - Fe_2O_3 ellipsoids.

quasi-elliptic structure of α - Fe_2O_3 evolved into regular ellipsoids with coarse surfaces (Fig. 7d). For a reaction time of 12 h, monodisperse and uniform ellipsoids could be produced, and craterlets in the surface of ellipsoids could be observed (Fig. 7e and the inset). The detailed characteristics of them were described previously. Therefore, the formation process of the porous α - Fe_2O_3 ellipsoids can be schematically illustrated in Fig. 7f. As can be seen, in the first stage of reaction, the nanoparticles were generated through hydrolysis. With prolonged hydrothermal treatment, the solid elliptic aggregates were formed by oriented attachment of these nanoparticles to minimize the overall surface energies of the system. Further increasing the hydrothermal time, these solid ellipsoids were subject to inside-out ripening. This evacuation process could initiate at regions near the surface depending on the ripening characteristics of the chemical species,³⁵ which led to porous or

hollow nanostructures. On the basis of the above analysis, it is believed that Ostwald ripening should be the main formation mechanism for the porous ellipsoids. It should be mentioned that a similar mechanism was also proposed for hydrothermal preparation of oxides with porous or hollow nanostructures.³⁶

Chemical sensors play a very important role in chemical industries, environmental protection, public safety, and human health.³⁷ Therefore, to demonstrate the potential application, a gas sensor based on porous α -Fe₂O₃ ellipsoids prepared with 0.2 g HMT at 160 °C for 12 h was fabricated and its gas sensing performances were investigated. Fig. 8a shows a bar graph of the response of the sensor to a variety of gases, such as ethanol, acetone, methanol, *etc.* All of the gases were tested at an operating temperature of 250 °C with a concentration of 100 ppm. It can be seen that the sensor exhibited the highest response to ethanol among the tested gases and the response was 25.6. Therefore, it is concluded that the sensor using porous α -Fe₂O₃ ellipsoids shows a selectivity toward ethanol as oppose to any other gas. It is well known that the response of a gas sensor is highly influenced by its operating temperature.³⁸ In order to determine the optimum operating temperature, the response of the sensor to 100 ppm ethanol and acetone were investigated as function of operating temperature, as shown in Fig. 8b. It is

obvious that the response to both tested gases varied with operating temperature. The response to ethanol first increased with temperature, up to 250 °C, and then gradually decreased. For acetone, the response continuously increased when operating temperature varied from 200 to 263 °C, and then decreased. The maximum response to acetone obtained was 16.7 at 263 °C. Therefore, an operating temperature of 250 and 263 °C were chosen for ethanol and acetone respectively, to further examine the characteristics of the gas sensor. The relationship between response and ethanol and acetone concentrations for the sensor at an operating temperature of 250 °C is displayed in Fig. 8c. From the two curves, it is clear that the response of sensor increased with the gas concentrations. The response did not exhibit significant difference for the two test gas. Moreover, the responses were proportional to the increasing concentrations of ethanol/acetone, when the gas concentrations were correspondingly low (the inset in Fig. 8c). As the gas concentrations increase, the increase of the response to ethanol was faster. Above 2000 ppm, the responses increased slowly with the gas concentrations, which indicated that the sensor tended to saturation gradually. For a gas sensor, the response and recovery times are also important parameters. Rapid response and recovery to a target gas are demanded for practical application.

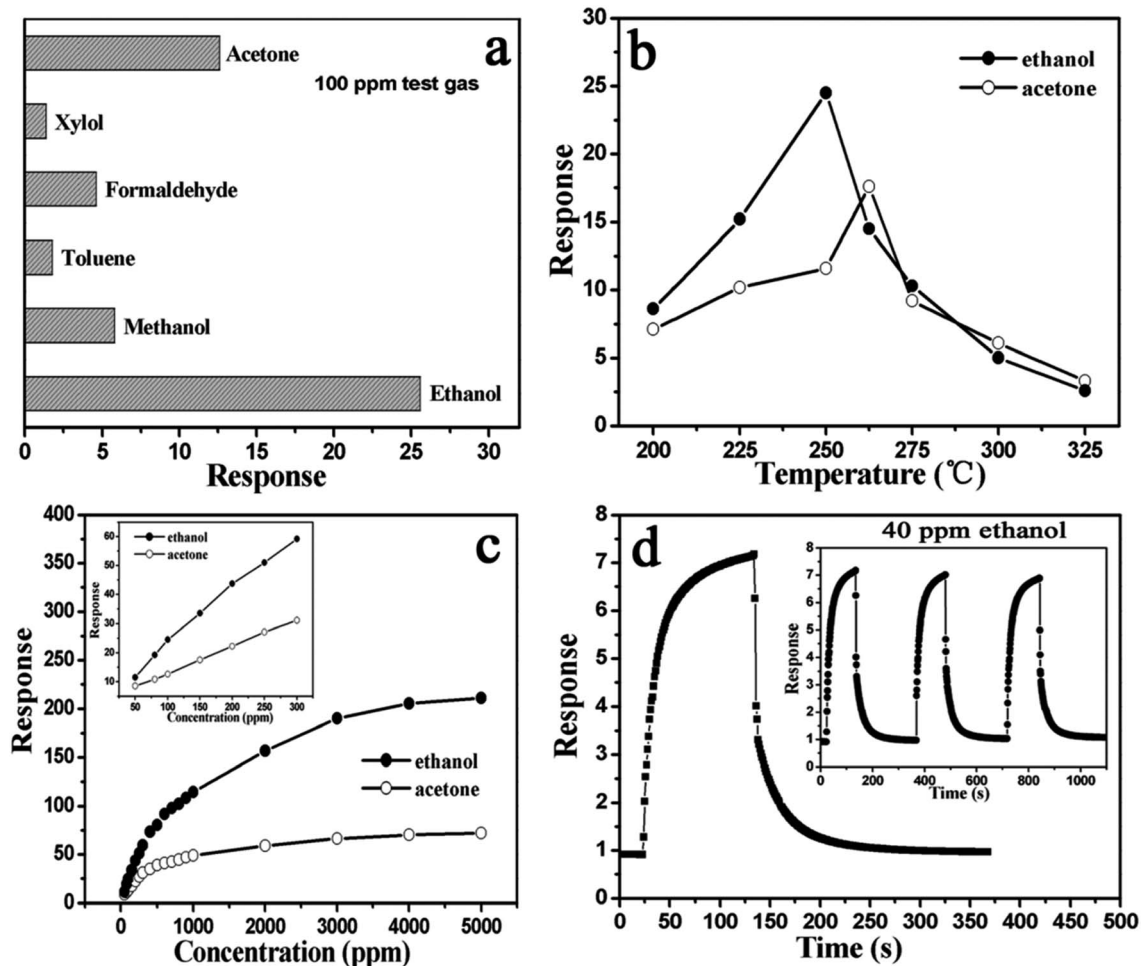


Fig. 8 (a) Response of the sensor to various test gases at 250 °C. (b) Response of the sensor to 100 ppm acetone and ethanol as a function of operating temperature. (c) Response *versus* ethanol and acetone concentrations at 250 °C. (d) Response transient of the sensor to 40 ppm ethanol.

Fig. 8d shows the response transients of the sensor to 40 ppm ethanol at 250 °C. The results indicate that the sensor immediately responded when ethanol was introduced. The response and recovery times of the sensor using as-prepared porous α -Fe₂O₃ ellipsoids were 38 and 34 s, respectively. The three reversible cycles of the response curve indicated a stable and repeatable characteristic, as shown in the inset of Fig. 8d.

The sensing mechanism of metal oxides has been clarified in previous works. The most widely accepted model is based on the change in resistance of the sensor upon exposure to different gas atmospheres.³⁹ When the sensor based on as-prepared porous α -Fe₂O₃ ellipsoids is exposed to air, oxygen molecules adsorb onto the surfaces of ellipsoids, and form chemisorbed oxygen species by capturing electrons from the conduction band of α -Fe₂O₃. The decrease of the electron concentration in the conduction band leads to stabilization of high surface resistance. When the sensor is exposed to ethanol, acetone, or other reductive gas atmospheres at a moderate temperature, these gas molecules will react with the adsorbed oxygen species on its surfaces. This process releases the trapped electrons back to the conduction band of α -Fe₂O₃ and results in an increase in the electron concentration. This effect eventually increases the conductivity of the porous α -Fe₂O₃ ellipsoids. The high response of the α -Fe₂O₃ ellipsoids gas sensor to ethanol is attributed to their unique architectures. Porous structures enable gas to diffuse easily into the interior of α -Fe₂O₃ ellipsoids. Therefore, when the porous α -Fe₂O₃ ellipsoid sensor is exposed to reducing gas, not only is the resistance of the particles near the surface of the ellipsoids affected, but also the particles in the core of ellipsoids become active. In other words, the utilization rate of the sensitive body is increased. This is the main reason for the high gas response in the porous α -Fe₂O₃ ellipsoids.

Conclusions

In summary, porous α -Fe₂O₃ nanostructures are synthesized by a simple one-step template-free method. This method is based on hydrothermal treatment of ferric trichloride in a mixed solvent of ethanol–water. The current method is suitable for inexpensive, large scale synthesis α -Fe₂O₃ porous ellipsoids. The inside-out Ostwald ripening mechanism is proposed to account for the template-free formation of these porous nanostructures. The as-prepared α -Fe₂O₃ porous ellipsoids exhibit superior gas sensing performance when used as sensing materials in gas sensing sensor.

Acknowledgements

This work was supported by NSFC (No. 61074172, 61134010, 61006055) and Program for Changjiang Scholars and Innovative Research Team in University (No. IRT1017) and Jilin province science and technology development plan program (20106002).

References

- J. Chen, L. N. Xu, W. Y. Li and X. L. Gou, *Adv. Mater.*, 2005, **17**, 582.
- J. S. Han, T. Bredow, D. E. Davey, A. B. Yu and D. E. Mulcahy, *Sens. Actuators, B*, 2001, **75**, 18.
- E. Comini, V. Guidi, C. Frigeri, I. Ricco and G. Sberveglieri, *Sens. Actuators, B*, 2001, **77**, 16.
- E. V. Shevchenko, D. V. Talapin, H. Schnablegger, A. Kornowski, O. Festin, P. Svedlindh, M. Haase and H. Weller, *J. Am. Chem. Soc.*, 2003, **125**, 9090.
- M. V. Tsodikov, T. N. Rostovshchikova, V. V. Smirnov, O. I. Kiseleva, Y. V. Maksimov, I. P. Suzdalev and V. N. Ikorskii, *Catal. Today*, 2005, **105**, 634.
- I. Cesar, A. Kay, J. A. Gonzalez Martinez and M. Grätzel, *J. Am. Chem. Soc.*, 2006, **128**, 4582.
- L. M. Bronstein, X. L. Huang, J. Retrum, A. Schmucker, M. Pink, B. D. Stein and B. Dragnea, *Chem. Mater.*, 2007, **19**, 3624.
- Y. M. Zhao, Y. H. Li, R. Z. Ma, M. J. Roe, D. G. McCartney and Y. Q. Zhu, *Small*, 2006, **2**, 422.
- Y. L. Chueh, M. W. Lai, J. Q. Liang, L. J. Chou and Z. L. Wang, *Adv. Funct. Mater.*, 2006, **16**, 2243.
- Z. Q. Liu, D. H. Zhang, S. Han, C. Li, B. Lei, W. G. Lu, J. Y. Fang and C. W. Zhou, *J. Am. Chem. Soc.*, 2005, **127**, 6.
- X. Hu, J. C. Yu, J. Gong, Q. Li and G. Li, *Adv. Mater.*, 2007, **19**, 2324.
- M. F. Casula, Y. W. Jun, D. J. Zaziski, E. M. Chan, A. Corrias and A. P. Alivisatos, *J. Am. Chem. Soc.*, 2006, **128**, 1675.
- Y. H. Ni, X. W. Ge, Z. C. Zhang and Q. Ye, *Chem. Mater.*, 2002, **14**, 1048.
- L. P. Zhu, H. M. Xiao, X. M. Liu and S. Y. Fu, *J. Mater. Chem.*, 2006, **16**, 1794.
- M. H. Cao, T. F. Liu, S. Gao, G. B. Sun, X. L. Wu, C. W. Hu and Z. L. Wang, *Angew. Chem., Int. Ed.*, 2005, **44**, 4197.
- S. W. Kim, M. Kim, W. Y. Lee and T. Hyeon, *J. Am. Chem. Soc.*, 2002, **124**, 7642.
- X. M. Sun and Y. D. Li, *Angew. Chem., Int. Ed.*, 2004, **43**, 3827.
- P. R. Selvakannan and M. Sastry, *Chem. Commun.*, 2005, (13), 1684.
- F. Caruso, *Chem.–Eur. J.*, 2000, **6**, 413.
- Z. Y. Zhong, Y. D. Lin, B. Gates and Y. D. Xia, *Adv. Mater.*, 2000, **12**, 206.
- M. Yang, J. Ma, C. L. Zhang, Z. Z. Yang and Y. F. Lu, *Angew. Chem., Int. Ed.*, 2005, **44**, 6727.
- H. P. Liang, H. M. Zhang, J. S. Hu, Y. G. Guo, L. J. Wan and C. L. Bai, *Angew. Chem., Int. Ed.*, 2004, **43**, 1540.
- C. I. Zoldesi and A. Imhof, *Adv. Mater.*, 2005, **17**, 924.
- Q. Peng, Y. J. Dong and Y. D. Li, *Angew. Chem., Int. Ed.*, 2003, **42**, 3027.
- H. G. Yang and H. C. Zeng, *J. Phys. Chem. B*, 2004, **108**, 3492.
- Y. Chang, J. J. Teo and H. C. Zeng, *Langmuir*, 2005, **21**, 1074.
- B. Liu and H. C. Zeng, *Small*, 2005, **1**, 566.
- L. Zhou, W. Z. Wang, H. L. Xu and S. M. Sun, *Cryst. Growth Des.*, 2008, **8**, 3595.
- H. Y. Yu, J. G. Yu, S. W. Liu and S. Mann, *Chem. Mater.*, 2007, **19**, 4327.
- X. W. Lou, Y. Wang, C. Yuan, J. Y. Lee and L. A. Archer, *Adv. Mater.*, 2006, **18**, 1325.
- Y. D. Yin, R. M. Rioux, C. K. Erdonmez, S. Hughes, G. A. Somorjai and A. P. Alivisatos, *Science*, 2004, **304**, 711.
- R. K. Chiang and R. T. Chiang, *Inorg. Chem.*, 2007, **46**, 369.
- B. Liu and H. C. Zeng, *J. Am. Chem. Soc.*, 2004, **126**, 8124.
- H. G. Yang and H. C. Zeng, *Angew. Chem., Int. Ed.*, 2004, **43**, 5930–5933.
- H. G. Yang and H. C. Zeng, *Angew. Chem., Int. Ed.*, 2004, **43**, 5206.
- (a) H. C. Zeng, *J. Mater. Chem.*, 2006, **16**, 649; (b) J. Li and H. C. Zeng, *J. Am. Chem. Soc.*, 2007, **129**, 15839; (c) Y. Zhao and L. Jiang, *Adv. Mater.*, 2009, **21**, 3621.
- (a) L. J. Bie, X. N. Yan, J. Yin, Y. Q. Duan and Z. H. Yuan, *Sens. Actuators, B*, 2007, **126**, 604; (b) C. Z. Wu, P. Yin, X. Zhu, C. Z. Yang and Y. Xie, *J. Phys. Chem. B*, 2006, **110**, 17806; (c) J. F. Liu, X. Wang, Q. Peng and Y. D. Li, *Sens. Actuators, B*, 2006, **115**, 481.
- (a) V. R. Shinde, T. P. Gujar and C. D. Lokhande, *Sens. Actuators, B*, 2007, **123**, 701; (b) H. Gong, J. Q. Hu, J. H. Wang, C. H. Ong and F. R. Zhu, *Sens. Actuators, B*, 2006, **115**, 247.
- (a) Z. Gergintschew, H. Förster, J. Kositzka and D. Schipanski, *Sens. Actuators, B*, 1995, **25**, 170; (b) D. E. Williams, *Sens. Actuators, B*, 1999, **57**, 1; (c) H. Gong, Y. J. Wang, S. C. Teo and L. Huang, *Sens. Actuators, B*, 1999, **54**, 232; (d) G. Sberveglieri, C. Baratto, E. Comini, G. Faglia, M. Ferroni, A. Ponzoni and A. Vomiero, *Sens. Actuators, B*, 2007, **121**, 208.